Biomaterials Advances 133 (2022) 112593

Contents lists available at ScienceDirect

Biomaterials Advances

journal homepage: www.elsevier.com/locate/bioadv

Maltodextrin-amino acids electrospun scaffolds cross-linked with Maillard-type reaction for skin tissue engineering

Marco Ruggeri [a], Eleonora Bianchi [a], Silvia Rossi [a], Cinzia Boselli [a], Antonia Icaro Cornaglia [b], Lorenzo Malavasi [c], Riccardo Carzino [d], Giulia Suarato [d], Rita Sánchez-Espejo [e,f], Athanassia Athanassiou [d], Cesar Viseras [e,f], Franca Ferrari [a], Giuseppina Sandri [a,*]

[a] Department of Drug Sciences, University of Pavia, Viale Taramelli 12, 27100 Pavia, Italy
[b] Department of Public Health, Experimental and Forensic Medicine, University of Pavia, via Forlanini 2, 27100 Pavia, Italy
[c] Department of Chemistry, University of Pavia, Viale Taramelli 14, 27100 Pavia, Italy
[d] Smart Materials, Istituto Italiano di Tecnologia, Via Morego 30, 16163 Genova, Italy
[e] Andalusian Institute of Earth Sciences, CSIC-UGR, Avenida de las Palmeras 4, Armilla, Granada 18100, Spain
[f] Department of Pharmacy and Pharmaceutical Technology, Faculty of Pharmacy, University of Granada, Campus of Cartuja, 18071 Granada, Spain

ARTICLE INFO

Keywords:
Chronic wounds
Maltodextrin
Amino acids
Maillard-type reaction
Mechanical properties
Surface zeta potential
Immune response
Murine burn/excisional model

ABSTRACT

The goal of this work is the design and the development of scaffolds based on maltodextrin (MD) to recover chronic lesions. MD was mixed with arginine/lysine/polylysine and the electrospinning was successfully used to prepare scaffolds with uniform and continuous nanofibers having regular shape and smooth surface. A thermal treatment was applied to obtain insoluble scaffolds in aqueous environment, taking the advantage of amino acids-polysaccharide conjugates formed via Maillard-type reaction. The morphological analysis showed that the scaffolds had nanofibrous structures, and that the cross-linking by heating did not significantly change the nanofibers' dimensions and did not alter the system stability. Moreover, the heating process caused a reduction of free amino group and proportionally increased scaffold cross-linking degree. The scaffolds were elastic and resistant to break, and possessed negative zeta potential in physiological fluids. These were characterized by direct antioxidant properties and Fe^{2+} chelation capability (indirect antioxidant properties). Moreover, the scaffolds were cytocompatible towards fibroblasts and monocytes-derived macrophages, and did not show any significant pro-inflammatory activity. Finally, those proved to accelerate the recovery of the burn/excisional wounds. Considering all the features, MD-poly/amino acids scaffolds could be considered as promising medical devices for the treatment of chronic wounds.

1. Introduction

Wound healing is a dynamic and regulated process involving a complex series of overlapping events, which are hemostasis, inflammatory, proliferative and remodeling stages. In chronic wounds, as venous and arterial ulcers, diabetic and pressure ulcers, the healing process does not lead to anatomical and functional recovery. Polysaccharides, such as chitin, chitosan, cellulose, hyaluronan, and alginate, have been widely proposed as biomaterials to enhance healing process thanks to their biocompatibility, low toxicity, and pharmaceutical biomedical activity. The rationale for their use is due to their antimicrobial effect and capability to reduce wound exudate, inflammation, and edema, and to promote wound reparation [1].

Maltodextrin (MD) is a D-glucose polysaccharide produced from vegetable starch by partial hydrolysis. In this work it has been selected as a potential wound healing agent due to its ability to promote fibroblasts proliferation [2].

Low dextrose equivalent (low content of reducing sugar and higher molecular weight) MDs are preferred as wound healing agents due to the higher content of longer polymeric chains, since these are able to form a film at the lesion site in contact to the granulation tissue and should avoid the loss of fluid and protect this site against pathogen colonization [3]. Moreover, MD seems to provide a high local nutrient supply, due to the degradation and the consequent gradual release of glucose to the wound [4]. However, water solubility impairs polysaccharide potential application in wound healing because of the short residence in the wound bed. For this reason, to improve the performance of polysaccharide-based systems, a cross-linking agent is needed. Together with the increase of resistance to water, polysaccharides cross-linking, which usually involves hydroxyl and/or carboxyl groups, reduces the chain mobility and improves

* Corresponding author.
E-mail address: g.sandri@unipv.it (G. Sandri).

http://dx.doi.org/10.1016/j.msec.2021.112593
Received 30 July 2021; Received in revised form 12 November 2021; Accepted 30 November 2021
Available online 3 December 2021

system mechanical strength, biocompatibility and tissue-like properties [5].

The formation of amino acids-polysaccharides conjugates via Maillard-type reaction is an alternative to toxic and expensive cross-linking agents. The reaction starts with the condensation between electrophilic carbonyl groups of polysaccharides and free amino groups of amino acids, peptides and proteins (especially the basic residues), forming a non-stable Schiff base, followed by Amadori rearrangement to form reactive α-carbonyl species capable of reacting with additional nucleophiles such as other amines and guanidines [6].

Further condensation reactions lead to the formation of a variety of advanced glycation end products (AGEs) and large heterogeneous polymeric compounds melanoidins, named also browning compounds (general schematic of the reaction in SI, Fig. S2) [7].

Interestingly, it has been reported that melanoidins possess a strong antioxidant activity, due to their ability to trap positively charged metabolites, scavenge oxygen radicals or chelate metals, particularly iron ions, to form inactive complexes [8]. In fact, in chronic wounds, reactive oxygen species (ROS) are released during the inflammation phase, leading to tissue damage and to increased expression of matrix metalloproteases and inflammatory cytokines [9]. Furthermore, iron ions magnify the oxidative stress processes: labile iron pool (LIP), especially Fe^{2+}, reacts with ROS such as superoxide anion and hydrogen peroxide, giving rise to hydroxyl radicals via the Fenton reaction or superoxide-driven Fenton chemistry [10].

Given these premises, the aim of this study was the design and the development of electrospun nanofibrous scaffolds, based on MD and α amino acids or its homopolymer thermally cross-linked via Maillard-type reaction, as dermal substitute for reparation and regeneration of chronic lesions or burns. This innovative approach allowed to consolidate a 3D nanofibrous structure of the scaffolds without chemicals and solvents with a sustainable and green process. Arginine (Arg) and Lysine (Lys), essential basic α amino acids particularly prone to react via Maillard reaction [11], with a peculiar function in the wound healing process were chosen. Moreover, a homopolymer of Lys, Polylysine (ε-polylysine) (PL), has been selected to highlight if the polymer-to-polymer interactions (MD-PL) could further stabilize the scaffolds 3D structure increasing the degree of polymerization of the Maillard-type reaction products [12]. In particular, Arg plays an important role in cell division and in immune response by means of an indirect mechanism via T cells stimulation directly related to enhanced fibroblasts activity [13]. It is also a precursor for the synthesis of nitric oxide through inducible nitric oxide synthase (iNOS) and it regulates collagen formation, cell proliferation and wound contraction. Lys has a crucial role in proteinogenesis and protein structure organization, especially in collagen and structural proteins of connective tissues, often lacking in chronic wounds [14]. ε-polylysine is a basic natural polymer of lysine, produced by *Streptomyces albulus*, well known as attachment factor to improve cell adhesion. It possesses antimicrobial properties, induces antiinflammatory reaction and consequently promotes wound healing [15–17].

The scaffolds were characterized by a multidisciplinary approach. The chemico-physical characterization involved system morphology, spectroscopic and thermal investigations, cross-linking degree, mechanical properties and surface zeta potential. Moreover, biopharmaceutical evaluation was performed considering direct and indirect antioxidant properties, biocompatibility towards fibroblasts and in vitro proinflammatory activity in macrophages model. Finally, efficacy and safety were assessed by means of an in vivo murine burn excisional model.

2. Materials and methods

2.1. Materials

MD (Glucidex 2, Roquette, Giusto Faravelli, Italy) was used as polysaccharide (molecular mass: 8589 g/mol; degree of polymerization: 52.9; dextrose equivalent value: 2) [18]. Lys homopolymer: PL (εPL, ε- poly- L-lysine, (MW 4.7 kDa, Epsiliseen®-H, Food Grade, Siveele B.V. AVG srl, Italy), α amino acids: Lys (L-lysine monohydrochloride, from non-animal source, EP, JP, USP compliant, Sigma-Aldrich, Italy) and Arg (L-arginine from non-animal source, EP, USP compliant, Sigma-Aldrich, Italy) were used as poly/amino acids. In Fig. S1 the chemical structures of materials are reported.

2.2. Methods

2.2.1. Preparation of electrospun scaffolds

Fig. 1a reports the composition of the polymeric blends (% *w*/w) and the electrospinning parameters used to obtain the corresponding scaffolds. MD-poly/amino acids were solubilized in distilled water under stirring overnight at room temperature. Pure MD solution was also prepared. The resulting blends were electrospun using a horizontal electrospinning apparatus equipped with a syringe having a metallic needle (inner diameter of 0.7 mm) (STKIT-40, Linari Engineering, Italy). A syringe pump was used to feed the blend at a constant rate. High voltage at the needle was achieved by connection to a voltage generator (Model R-99E, Razel TM, Italy). A plastic stand wrapped with an aluminum foil was used as planar collector. The relative humidity and the environmental temperature were set at 30–40% and 25 °C, respectively. Scaffolds were cross-linked by heating at 180 °C for 2 h. This process is also reported as able to dry sterilize the products (Ph. Eur. X edition, methods of preparation of sterile products).

2.2.2. Chemico-physical characterization

The nanofiber morphology was assessed by means of SEM (Mira3XMU, Tescan, Czech Republic), after graphite sputtering. The morphology of the scaffolds was analyzed before, after cross-linking, and after hydration. The nanofiber diameters and their size distribution (in SI) were measured by means of an image analysis software (Image J, ICY, Institute Pasteur, France).

Fourier-transform infrared spectroscopy (FT-IR) spectra of the powdery samples were obtained with a JASCO 6200 apparatus (USA) equipped with a Ge ATR. All analyses were performed from 400 to 4000 cm^{-1} with a resolution of 2 cm^{-1}, and results processed with Spectra Manager v2 software. The FT-IR spectra were smoothed, and the noise was removed using the Savitzky-Golay filter (OriginPro 2021b, OriginLab Corporation).

X-ray photoelectron spectroscopy (XPS) was performed using an electron spectrometer (Lab2, Specs, Greece) equipped with a monochromatic X-ray source (set at 1486 eV) and with a hemispherical energy analyzer (Phoibos, HSA3500, Specs, Greece) (detailed in SI).

Thermogravimetric analysis (TGA) was performed using a system (Shimadzu, mod. TGA-50H, England), equipped with a vertical oven and a precision of 0.001 mg. Approximately 40 mg of each sample were weighted in aluminum sample pans. The experiments were performed in 30–950 °C range, atmospheric air, and a heating rate of 10 °C/min. Additionally, differential scanning calorimetry (DSC) analyses were performed (Mettler Toledo, England) using aluminum crucibles in a temperature range between 30 and 400 °C at a heating rate of 10 °C/min. All the analyses were done in atmospheric air.

2.2.3. Cross-linking degree and in vitro degradation

The cross-linking degree of the scaffolds was determined using ninhydrin assay [19]. At this purpose, samples (10 mg) were subjected to heating at 180 °C for different times up to 120 min. Then, the samples were hydrated in distilled water (3 mL), stirred for 3 min at room temperature and centrifuged at 3000*g* for 10 min. The supernatant was assayed using ninhydrin (described in SI), and the absorbance read at 570 nm (ELISA plate reader, Biorad, Italy). The pure MD scaffolds was also characterized and considered the negative control. The signal obtained for this (0.131 AU ± 0.029) was subtracted to all the other samples assayed. The calibration curves of Arg (0.4–0.02 mg/mL), PL (0.28–0.013 mg/mL) and Lys (0.9–0.05 mg/mL) were linear with R^2 values always higher than 0.995. Each measurement was at least duplicated.

To evaluate the scaffold degradation, each scaffold (about 10 mg) was weighed (W_i) and placed in 6 mL of PBS (phosphate saline buffer pH 7.4,

a)

% w/w	MD	Arg	Lys	PL	V	N/C	Flow
MD Arg 10:1	47	4.7			25	20	0.569
MD Arg 8:1	47	5.8			25	20	0.569
MD Lys 6:1	47		7.83		20	23	0.947
MD Lys 4:1	47		11.85		20	23	0.947
MD PL 30:1	47			1.57	20	20	0.947
MD PL 19:1	47			2.47	20	20	0.947
MD	47				20	20	0.947

b)

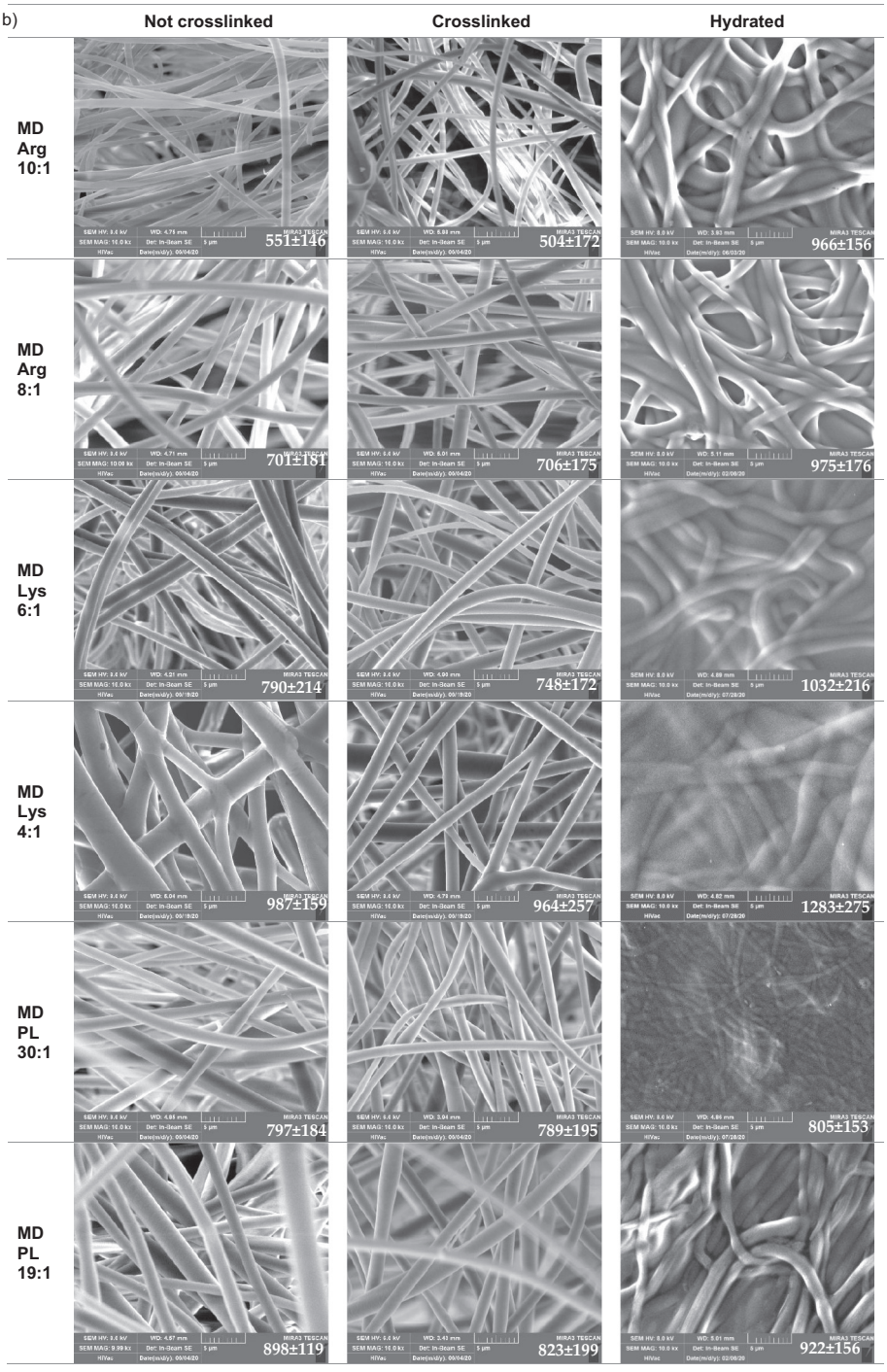

Fig. 1. a) Composition (% *w*/w) of polymeric blends (MD:maltodextrin; Arg: arginine; Lys: lysine; PL: polylysine) and electrospinning parameters (V: voltage-kV; N/C: needle to collector distance-cm; Flow-mL/h); b) SEM micrographs of scaffolds immediately after preparation (not cross-linked), after cross-linking and after 6 days of hydration in water. In each image the diameters (nm) are reported (mean values ± sd; $n = 100$).

Sigma-Aldrich, Italy) at 37 °C. Samples were removed after 3 and 6 days from the solution, wiped with a paper, left to dry at room temperature for 2 h and reweighed (W_f), and the weight loss was calculated as follows:

$$\text{Weight loss } (\%) = \frac{W_i - W_f}{W_i} * 100 \quad (1)$$

2.2.4. Determination of the formation of Maillard-type reaction products (intermediate and browning compounds)

To monitor Maillard-type reaction during dry-heating, samples (10 mg) were subjected to heating at 180 °C for different times up to 120 min. The samples were hydrated in distilled water (3 mL), stirred for 3 min at room temperature and centrifuged at 3000*g* for 10 min before absorbance measurements. The intermediate and browning compounds formation was determined by the absorbance of the supernatants at 304 and 420 nm (Lamba 25, Perkin Elmer, Italy), respectively [7]. Sample dilution was performed to obtain an absorbance always lower than 1 AU. Each measurement was at least duplicated.

2.2.5. Assessment of fiber mechanical properties

Mechanical properties of nanofibrous scaffolds were measured using a dynamometer (TA-XT plus, Stable Microsystems, Italy) equipped with a 5.0 kg load cell. Before testing, nanofibrous scaffolds were cut 30 × 10 mm and the strips were clamped between two tensile grips (A/TG probe) setting an initial distance between the grips of 20.0 mm. Then, the upper grip was moved forward at a constant speed of 5.0 mm/s up to break. Mechanical properties were evaluated in dry and hydrated state, and force at break vs. distance was recorded, and the elongation and Young modulus were calculated [20]. Each measurement was at least duplicated.

2.2.6. Surface zeta potential

The apparent zeta potential (ζ) of each scaffold was determined from the measurement of the streaming potential. Streaming potential measurements were performed with SurPASS™ 3 (Anton Paar GmbH, Italy) using the cylindrical cell. The scaffolds (10 × 10 mm^2) were mounted dry between two filter disks in the sample holder of the cylindrical cell. 0.1 mol/L KCl aqueous solution was used as the streaming solvent and its pH was scanned in the range 2–9, to determine the isoelectric point (pI) and the ζ at physiological pH [21,22]. Each measurement was at least duplicated.

2.2.7. DPPH radical scavenging assay and ferrous ion chelating ability

For time-dependent assay, 10 mg scaffolds were placed in 6 mL of PBS at 37 °C to simulate the scaffold implant in the lesion bed. At prefixed times, the supernatants were collected, and each sample was divided in two aliquots. One aliquot was assayed to quantify the DPPH activity (direct antioxidant properties) and, for this purpose, each sample (1 mL) was mixed with 1 mL of DPPH methanol solution (8 μg/mL), kept 30 min in the dark and the absorbance measured at 515 nm (Lamba 25, Perkin Elmer, Italy) [23]. The results were expressed as gallic acid equivalents (μg GA/mg sample), and DPPH radical scavenging activity was calculated using the following expression:

$$\text{DPPH scavenging activity } \left(\%/\text{mg}^{-1} \cdot \text{ml}\right) = \left(\frac{A_{sample} - A_{blank}}{A_{control}}\right) \times \left(\frac{100}{\text{mg}^{-1}.\text{ml}_{sample}}\right) \quad (2)$$

The second aliquot was assayed to quantify the scaffold chelating activity towards ferrous ion (Fe^{2+}) (indirect antioxidant properties) by measuring the decrease in absorbance at 562 nm of the iron (II)–ferrozine complex [24]. For this purpose, 0.125 mM $FeCl_2$ solution (0.5 mL) was mixed 1:1 volume ratio with the sample, and then 0.3125 mM ferrozine (1 mL) was added. The mixtures were left to equilibrate at room temperature for 10 min. The absorbance was measured at 562 nm against the blank (sample before the reaction) and the results were expressed as EDTA equivalents (μg EDTA/mg sample). The ability of the scaffolds to chelate Fe^{2+} was calculated using the following expression:

$$\text{Ferrous ion chelating activity } \left(\%/\text{mg}^{-1} \cdot \text{ml}\right) = \left(\frac{A_{sample} - A_{blank}}{A_{control}}\right) \times \left(\frac{100}{\text{mg}^{-1}.\text{ml}_{sample}}\right) \quad (3)$$

The calibration curves of GA (6.84–0.34 μg/mL) and EDTA (117–5.85 μg/mL) were linear with R^2 values always higher than 0.9964. Each measurement was at least duplicated.

2.2.8. In vitro evaluation of scaffolds

2.2.8.1. Cytocompatibility of fibroblasts. The scaffold cytotoxicity was evaluated from the ISO standard test method (ISO 10993-5:2009, biological evaluation of medical devices). Each scaffold (10 mg) was sterilized by UV radiation for 15 min and then incubated in a serum-free DMEM medium (Dulbecco's Modified Eagle's Medium, PromoCell, WVR, Italy) for 24 h to produce extraction media of different concentrations (10.0, 7.5, 5.0 and 2.5 mg/mL). Normal human dermal fibroblast cells (NHDFs from juvenile foreskin, PromoCell, WVR, Italy) were cultured in DMEM medium (Sigma-Aldrich, Italy) supplemented with 200 IU/mL penicillin/0.2 mg/mL (Sigma-Aldrich, Italy) and with 10% fetal bovine serum (FBS, Euroclone, Italy). Fibroblasts were seeded at a density of $35*10^3$ cells/well in 96-well plate and, when the cultures reached confluency, the extraction media were added, and fibroblasts re-incubated for 24 h. After 24 h, the MTT [3-(4,5-dimethylthiazol-2-yl)-2,5-diphenyltetrazolium bromide] assay was performed. The medium in each well was removed and 100 μL of MTT solution at 1 mg/mL in DMEM w/o phenol red (Sigma-Aldrich, Milan, Italy) were added. Then, the cells substrates were placed at 37 °C for 3 h in incubator, and finally, MTT solution was removed and 100 μl of isopropanol (Carlo Erba, Italy) was added and the absorbance read using FLUOstar® Omega Microplate Reader (BMG LABTECH, Italy) at λ = 570 nm (with reference λ = 690 nm). Each measurement was at least duplicated.

2.2.8.2. Cytocompatibility of macrophages and pro-inflammatory immune response. hMoCD14 + -PB-c cell line, human CD14+ monocytes derived from peripheral blood, (Carlo Erba, Italy) was cultured in mononuclear cell medium (Carlo Erba, Italy) supplemented with 10% fetal bovine serum (FBS, Euroclone, Italy), and with 200 IU/mL penicillin/0.2 mg/mL streptomycin (Sigma-Aldrich, Italy) kept at 37 °C in a 5% CO_2 atmosphere with 95% relative humidity (RH). hMoCD14 + -PB-c were seeded 20 × 10^3 cells/well in a 24-well transwell and incubated for 72 h with 100 nM for $1*10^5$ cells of phorbol 12-myristate-13-acetate (PMA, Sigma-Aldrich, Italy) to allow differentiation. After differentiation, scaffolds were placed in the upper chamber and after 24 h of contact time, the scaffold cytocompatibility was assessed using Alamar Blue (Thermo Fisher Scientific, Italy) assay. The growth medium was removed from the wells, 100 μL of a AlamarBlue solution (10% *w*/w in DMEM w/o phenol red) were poured in each well, and then the well plate was placed in an incubator at 37 °C for 3 h. The AlamarBlue solution (100 μL) was then withdrawn, put in a different 96-well plate and the absorbance was detected using FLUOstar® Omega Microplate Reader at two different wavelengths: 570 nm, which is able to detect the reduced form (red) of the AlamarBlue, and 655 nm, which is able to detect the oxidized form (blue) of the AlamarBlue.

TNF-α, pro-inflammatory cytokine, was assayed to evaluate the pro-inflammatory immune response using the ELISA kit (Thermo Fisher, Italy). Supernatants were collected from the cultures after 24 h of treatment with the scaffolds and the cytokine secretion by macrophages was assayed at 450 nm with 570 nm as the reference wavelength. The method was linear in the concentration range from 7.8 to 500 pg/mL with the R^2 always higher than 0.995. Lipopolysaccharide (LPS, 2 μg/mL for 24 h) was used as positive control [25]. Each measurement was at least duplicated.

2.2.9. In vivo wound healing studies

All animal experiments were carried out in full compliance with the standard international ethical guidelines (European Communities Council Directive 86/609/EEC) approved by Italian Health Ministry (D.L. 116/92). The study protocol was approved by the Local Institutional Ethics Committee of the University of Pavia for the use of animals and by ISS (Istituto Superiore di Sanità). Nine male rats (Wistar 200–250 g, Envigo RMS S.r.l.) were anesthetized with equitensine at 3 mL/kg (39 mM pentobarbital, 256 mM chloral hydrate, 86 mM $MgSO_4$, 10% *v*/v ethanol, and 39.6% v/v propylene glycol) and shaved to remove all hair from their backs for the following evaluations. After, the treatments, all animals were then carefully monitored for the following 3 days by animal care services and received additional treatment of the same pharmacological treatments.

2.2.9.1. Evaluation of systems safety. Scaffolds having 4 mm diameter were subcutaneously implanted by means of an 8 mm incision (one for each rat) in the rats' back. The incisions were then sutured using strips (Steri-Strip Suture, Italy). After the treatment (1 + 17 days), full thickness biopsies were taken in correspondence of the incisions and the histological analysis was performed. A biopsy of intact skin was also taken for comparison.

2.2.9.2. Evaluation of systems efficacy on excisional/burn model. Three circular full thickness burns, 4 mm in diameter, were produced on the back of the animals by contact with an aluminum rod (105 °C for 40 s). After 24 h, the formed blisters were removed using a 4 mm diameter biopsy punch to obtain a full-thickness lesions. Scaffolds having 4 mm diameter (as big as the lesions) were applied and wetted with 20 μl of saline solution (0.9 g/l). Lesions treated with 20 μL of saline solution were the negative control. Lesions were covered with a sterile gauze and the rats' back was wrapped with a surgery stretch (Safety, Italy) to protect lesions. At prefixed times after blister removal (0, 3, 6, 10, 13 and 17 days) photographs of the lesions were taken by using a digital camera (Sigma SD 14) which allowed for sizing the lesions and monitoring the healing process. The size of wounded area was determined with an image analysis software (Image J, ICY, Institute Pasteur, France). Eighteen days after the treatment, full thickness biopsies were taken in correspondence of the initial lesions and the histological analysis of the excised tissues was performed. A biopsy of intact skin was also taken for comparison.

2.2.9.3. Histological analysis. Tissue samples were bisected along the wildest line of the wound, immediately immersed in the fixative solution (10% neutral buffered formalin), embedded in paraffin and sectioned at a thickness of 5 μm. Some sections were stained with hematoxylin and eosin (H&E), others with picrosirius red (PSR). Picrosirius red stain was applied as follows: deparaffinized sections were hydrated, faintly stained with Weigert's hematoxylin for nuclei, and stained with PSR (1 h). Then all sections were dehydrated, cleared in xylene and mounted with DPX. Stained sections were observed with a light microscope Carl Zeiss Axiophot provided, for circular polarising microscopy, with suitable filters in the condenser stage and in the microscope tube. Images were recorded through a microscope digital 5 megapixels CCD camera Nikon DS - Fi2.

2.2.10. Statistical analysis

Statistical analyses were performed using Astatsa statistical calculator. One-way analysis of variance (ANOVA) was followed by Scheffè for post-hoc comparisons. $p < 0.05$ was considered significant.

3. Results and discussion

3.1. Chemico-physical characterization

A pre-formulative study was performed. The threshold concentration required to generate a continuous polymeric solution jet during electrospinning (SI: entanglement concentration, Fig. S3) was 13% *w*/w, however, 47% w/w was the minimum concentration to obtain regular and homogenous nanofibers without defects. Two weight ratios between MD (at 47% *w*/w) and each poly/amino acid were considered on the basis of the spinnability of the resulting blends (no beads and ribbons). The surface tension, conductivity and viscosity of the polymeric blends play a pivotal role in the electrospinning process, since the surface tension affects the formation of Taylor's cone, and electrical charge and high viscosity of the solution favor the formation of bead-free fibers [27]. All the blends were characterized by similar values of surface tension, and as expected, their conductivity and their viscosity profiles increased with increasing poly/amino acids concentration (SI: Table S1 and Fig. S4).

All the polymeric blends (Fig. 1a) were electrospun and Fig. 1b reports SEM micrographs of MD-based scaffolds loaded with Arg, Lys, and PL at different weight ratios. In each image, the mean diameters (nm) are reported while Table S2 reports the diameter distributions. The morphological analysis shows that all the scaffolds had a nanofibrous structure independently from the poly/amino acids type and concentration. Cross-linking by heating did not significantly change the nanofibers' dimensions. In particular, scaffolds based on Arg were made of cylindrical and uniform fibers with smooth surfaces. Furthermore, the scaffolds retained the nanofibrous structure after hydration, showing a swelling of the individual fibers. The hydration of the scaffolds MD Arg 10:1 and MD Arg 8:1 caused an increase of the fibers' diameter from 504 ± 172 to 966 ± 156 nm and from 706 ± 175 to 975 ± 175 nm, respectively. Similar considerations are valid for scaffolds containing lysine or polylysine.

The fibers morphology at the dry state was regular and homogenous, while after the hydration the higher the poly/amino acid content (from MD Lys 6:1 to MD Lys 4:1 or from MD PL 30:1 to MD PL 19:1) the greater the swelling. The presence of Arg or Lys caused a significant increase in the fibers' dimensions upon swelling: MD Arg 10:1 swelled about 48% and MD Arg 8:1 about 28% while MD Lys 6:1 swelled about 28% and MD Lys 4:1 about 25%. Both the two polylysine-based scaffolds presented a minimal swelling (maximum 10%) and the fibers' dimensions before and after swelling were not significantly different. The heating treatment of the scaffolds induced the Maillard-type reaction between the poly/amino acids bearing amino groups and the reducing end of D-glucose carbonyl group (the basic unit of maltodextrin) (one active functional group per macromolecule) leading to glycoconjugates, *N*-glycosides. Amino groups of poly/amino acids react with the carbonyl function of glucose and form imines (Schiff bases), and those rearrange in amino ketoses, called Amadori compounds. These have a limited stability and in the 4–7 pH range degrade to 1-,3-, and 4-deoxydicarbonyl compounds (deoxyosones).

The condensation between nucleophilic/electrophilic intermediates of the Maillard-type reaction resulted in the formation of the brown components, called melanoidins. The reactive amino groups were the primary amino group of lysine and polylysine (pKa 10.53 and 10, respectively) and the guanidine group of arginine (pKa 12.48). Polylysine has multiple reactive amino groups, and this should consolidate the nanofiber morphology thanks to multiple condensation points with the same polylysine chain, causing a minimum change in fiber dimensions after hydration. This has also been observed in ε-polylysine–chitosan conjugates prepared via Maillard reaction [26].

Fig. 2a reports FTIR spectra of the scaffolds immediately after preparation (NC) and after cross-linking (C) for the three different amino acids. In the Fig. S5 the spectra of the pure components are reported. In general, the spectra of all the scaffolds (Fig. 2a) were dominated by the MD spectrum (Fig. S5 in SI), particularly for the low amino acids concentrations. For this reason, the investigation was performed on scaffolds containing the highest amino acids concentrations before and after the cross-linking, and these were compared with pure MD (lower MD:amino acids weight ratios not shown). The cross-linking process caused modification of the spectra that could be referred to the formation of melanoidins, due to the Maillard-type reaction. In particular, it was possible to observe a decrease of intensity of CN stretching in the region of 1250–1020 cm^{-1} (orange band), attributable to the NH_2 functional groups of the poly/amino acids consumption due to the crosslinking process. This was more pronounced in the scaffolds containing Lys and PL.

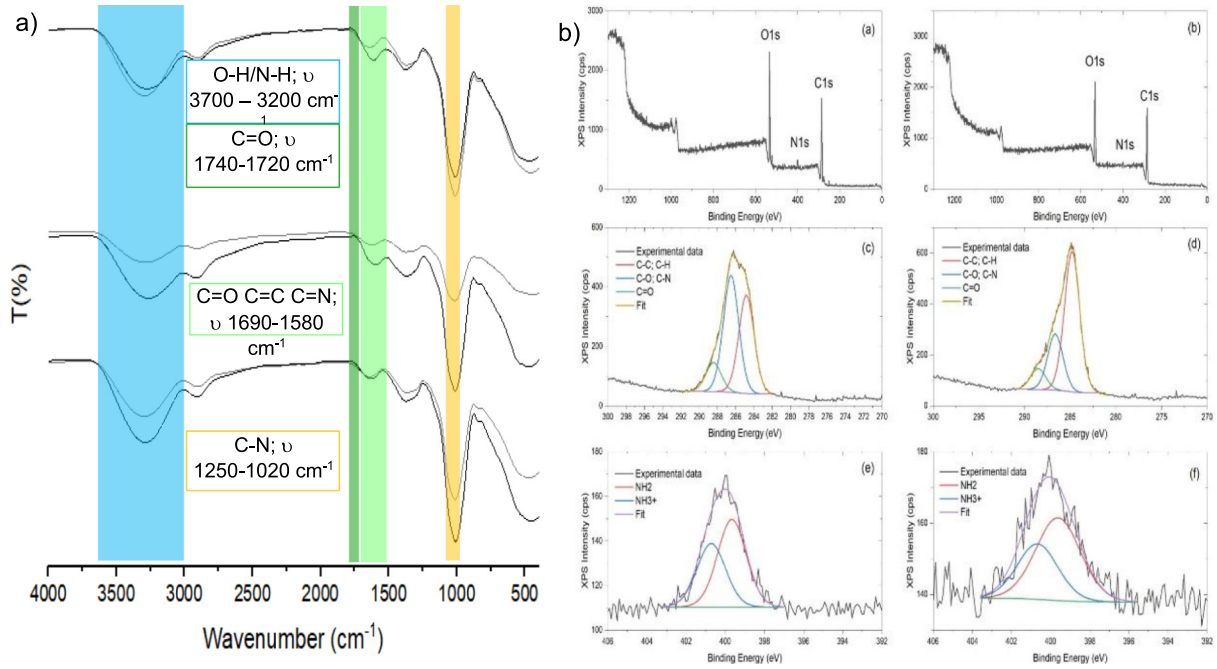

c)

At%	C1s		O1s		N1s		Cl2p		C-O; C-N/C-C		C=O/C-C		NH_2/NH_3^+	
Sample	nc	c	nc	c	nc	c	nc	c	nc	c	nc	c	nc	c
MD Arg 10:1	67.3	80.5	29.8	18.1	2.9	1.4	-	-	1.18	0.4	0.28	0.15	1.36	1.62
MD Arg 8:1	67.3	69.2	29.2	28.0	3.5	2.8	-	-	1.15	0.9	0.29	0.27	0.6	0.85
MD Lys 6:1	64.6	69.7	32.2	29.4	1.9	0.9	1.3	-	1.44	1.05	0.25	0.26	0.56	2.12
MD Lys 4:1	62.8	69.4	32.8	26.8	3.1	3.8	1.3	-	1.99	0.8	0.28	0.17	0.20	1.98
MD PL 30:1	69.7	76.9	27.8	22.3	2.5	0.8	-	-	0.98	0.62	0.25	0.15	1.63	0.68
MD PL 19:1	70.7	71.0	26.8	27.6	2.5	1.4	-	-	0.85	0.91	0.24	0.25	3.8	3.8

Fig. 2. a) FTIR spectra of scaffolds immediately after preparation (gray lines) and after cross-linking (black lines) for the three different amino acids (from top: lysine, arginine, and polylysine): 1250–1020 cm^{-1}: orange band; 1690–1580 cm^{-1}: green; 1740–1720 cm^{-1} dark green band; band; blue band; δ deformation/bending; υ stretching; (; b) XPS measurements performed on MD:Arg 10:1 scaffolds before (a,c,e) and after (b,d,f) Maillard-type reaction, (a,b) Wide scans respectively before and after the thermal treatment, (c,d) C1s and (e,f) N1s high resolution scans and decovolutions of the scaffolds before and after the thermal treatment; c) Element composition (Atomic%) on the scaffold surface determined by XPS analysis 233 (nc: not cross-linked; c: cross-linked).

In the region of 1690–1580 cm^{-1}, an increase of peak intensity appeared in the crosslinked scaffolds compared to the not cross linked ones. This is attributable to double bond stretching (C = O; C = C; CN) typical of the melanoidins, furthermore the appearance of a peak at 1690–1680 cm^{-1} typical of the stretching of melanoidin amide group has been masked by the decrease of NH peak (1650–1580 cm^{-1}) caused by amine bending (green band).

In the cross-linked scaffolds, in the region of 1740–1720 cm^{-1} (dark green band) a low intensity shoulder typical of IR fingerprint of the Amadori compounds (C = O) appeared indicating the presence of the open-chain sugar form [28].

In MD spectrum (Fig. S5), the region between 3200 and 3550 cm^{-1} was characterized by a wide peak corresponding to hydroxyl group stretching and this was present in all the spectra of the scaffolds before and after crosslinking. This totally hid the change in intensity of OH vibration at 3600–3200 cm^{-1} and that of amide NH stretch at 3700–3500 cm^{-1}, both typical of melanoidins in the crosslinked scaffolds (blue band).

To better understand the effect of the Maillard-type reaction on the scaffolds surfaces, XPS spectra were acquired (Fig. 2b and S6-S10). The wide scans and the high resolution C1s and N1s spectra of MD and Arg samples are reported as an example in Fig. 2b. The spectra differ significantly after Maillard-type reaction. After the thermal treatment the atomic content of carbon, oxygen and nitrogen changed; as reported in Fig. 2b, the atomic percentage of C1s increases from 67.3% to 80.5% while the oxygen and the nitrogen decrease from 29.8% to 18.1% and 2.9% to 1,4%, respectively. High resolution C1s spectrum exhibited the characteristic peaks C-C/C-H; C-O/C-N and CO at 248.8 eV, 286.5 eV and 288.5 eV, respectively. As clearly visible in Fig. 2b, the heating treatment causes a decrease of the C-O/C-N and CO peaks compared to the main carbon peak at 284.8 eV. At the same time, the peak at 399.6 eV assigned to unprotonated NH_2 group increases compared to the peak at 400,7 eV assigned to protonated NH_3^+ group.

All the calculated atomic percentage contents from the XPS spectra are reported (see Fig. 2c). All scaffolds showed similar behavior except from the one containing a higher amount of Lys. This atomic percentage changes at the fibers' surface could be related to the cross-linking degree and is considered a signal of the formation of Maillard-type reaction products. The oxygen reduction was probably due to water-loss occurring during the crosslinking process, while the significant decrease of nitrogen content could be related to the formation of volatile Maillard-type reaction products. Similar evidence was reported by Lee et al., which evaluated the volatile components formed via thermal reaction (180 °C for 90 min) between wheat gluten hydrolysates and glucose [29].

TGA profiles of the samples are shown in Fig. 3 (a-d). As for the pristine components (Fig. 3 a), both MD and PL (having a polymeric structure) showed weight loss in three stages with total carbonization at 500 °C (MD) or 600 °C (PL). MD thermal degradation profile showed a first small weight loss at around 100 °C assigned to evaporation of water (6.5% loss in weight) followed by an intense weight loss (73%) with maximum rate at 329 °C, corresponding to depolymerization of the polysaccharide and

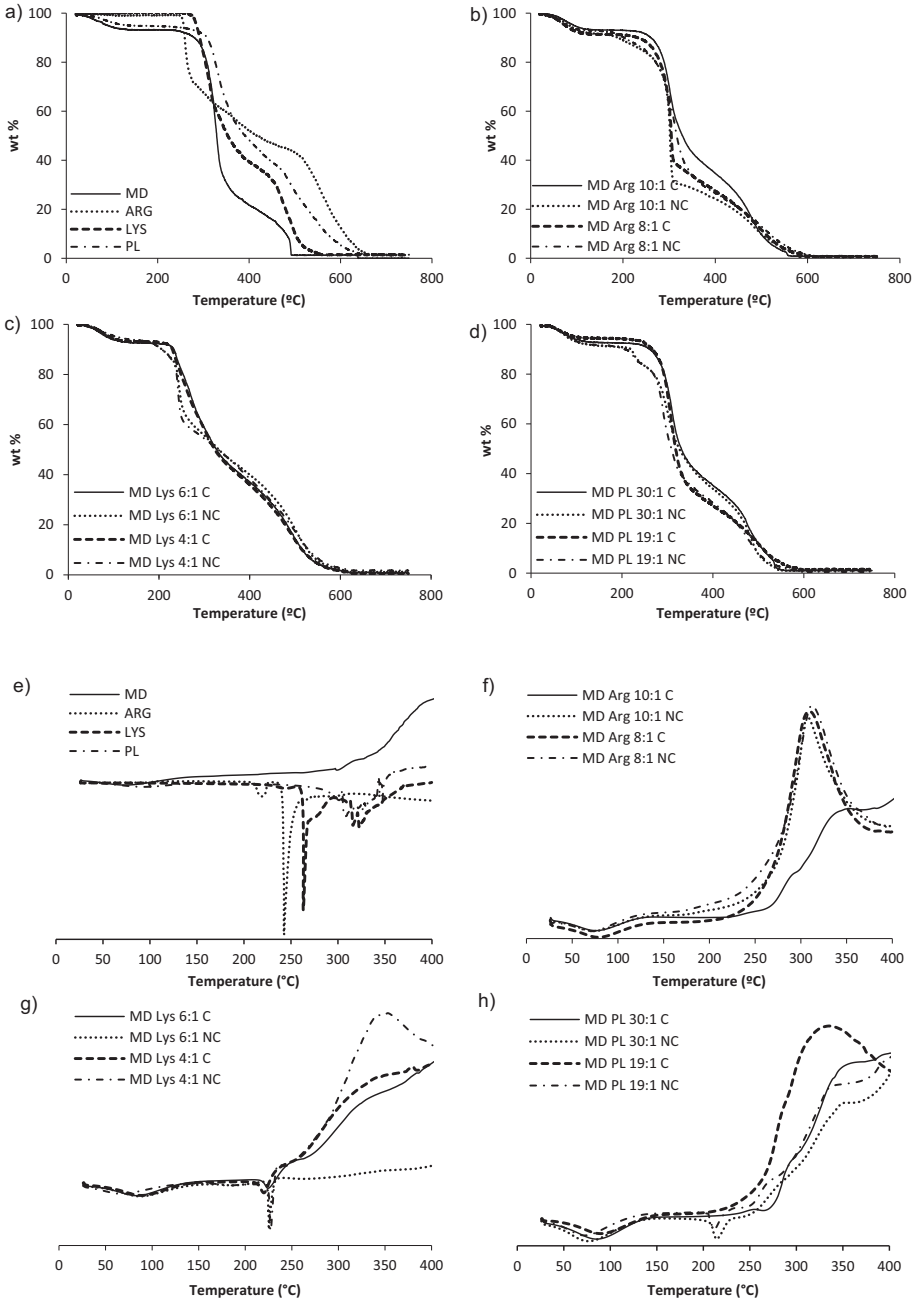

Fig. 3. Thermal analysis (TGA – a-d figures, and DSC – e-h figures) of pristine components and scaffolds.

loss of resultant volatile products. Finally, small residues oxidized to carbon dioxide at 490 °C. PL also showed a first humidity loss (5%) followed by depolymerization at 325 °C (48%) and almost continuous degradation of resultant residues up to 600 °C.

Arg and Lys TG curves showed two stages of weight loss. Both Lys and Arg were characterized by no weight loss up to 275 and 250 °C, respectively. The first stage of weight loss closed at 400 and 300 °C with 30 and 60%, respectively and the second stage closed at 560 and 660 °C, respectively.

All the scaffolds (Fig. 3 b-d) showed a first water loss followed by a two-stages degradation of the components. The first stage occurred in all the samples over 200 °C, with differences among the cross-linked (C) and not cross-linked (NC) scaffolds. In general, independently of the composition, the NC scaffolds showed a more intense and fast degradation stage, while NC scaffolds showed the same behavior although this was shifted to lower temperatures, suggesting that the cross-linked scaffolds were more stable to thermal degradation than the corresponding not crosslinked ones. The heating treatment required to cross-link the scaffolds via Maillard-type reaction, was able to increase thermal stability and this could be related to the Maillard-type reaction products. Nevertheless, the differences in temperature value corresponding to the maximum degradation rate for different samples were not significant.

DSC profiles (Fig. 3 e-h) of the samples corroborated the effective interaction between Arg, Lys and PL with MD via Maillard-type reaction. As for DSC curves of pristine materials (Fig. 3 e), MD did not show any endothermic peak, suggesting that the polymer was amorphous while Arg and Lys profiles showed intense melting peaks at 242 and 263 °C, respectively. Finally, all the crosslinked scaffolds, independently of the poly/amino acids, did not show Lys or Arg melting peaks or endothermic events related to PL and this is conceivably due to an intense interaction of poly/amino acids with MD involved in the Maillard-type reaction.

3.2. Cross-linking degree and in vitro degradation

Fig. 4 shows the percentage of the free amino groups (a) and the cross-linking degree (b) of scaffolds subjected to heating treatment at 180 °C for 120 min.

The increase of the cross-linking time decreased the percentage of free amino groups, and this is inversely related to the MD:poly/amino acids weight ratio (Fig. 4a). A steep reduction of free amino groups occurs after 30 min of heating and the scaffolds based on Arg (MD Arg 8:1 and MD Arg 10:1), MD PL 30:1 and MD Lys 6:1 reached plateau values, while scaffolds based on MD PL 19:1 and MD Lys 4:1 reacted slowly and reached the plateau values after 60–120 min. No significant difference was observed on the degree of cross-linking among the different scaffolds, except for MD PL 30:1 (vs. MD Arg 8:1 and MD Lys 6:1): these differences are probably due to the polylysine structure that became less flexible and less prone to interact as soon as the Maillard-type reaction proceeded, having multiple amino groups on the same macromolecules.

Fig. 4c reports the scaffold in vitro degradation in PBS at 37 °C. All the scaffolds were characterized by almost the same behavior independently from the poly/amino acid or the weight ratio. The scaffolds showed a weight loss of about 21–35% ($p < 0.05$) after 3 days and of about 42–56% after 6 days in PBS, although the scaffolds maintained their integrity (fibrous morphology) as shown in the SEM micrographs (Fig. 1b). In particular, MD PL 30:1 showed the highest weight loss, in accordance with the cross-linking degree. The cross-linking process is crucial for obtaining water resistant structure and for preserving the scaffold architecture in aqueous environment, since native scaffolds are prone to a fast dissolution.

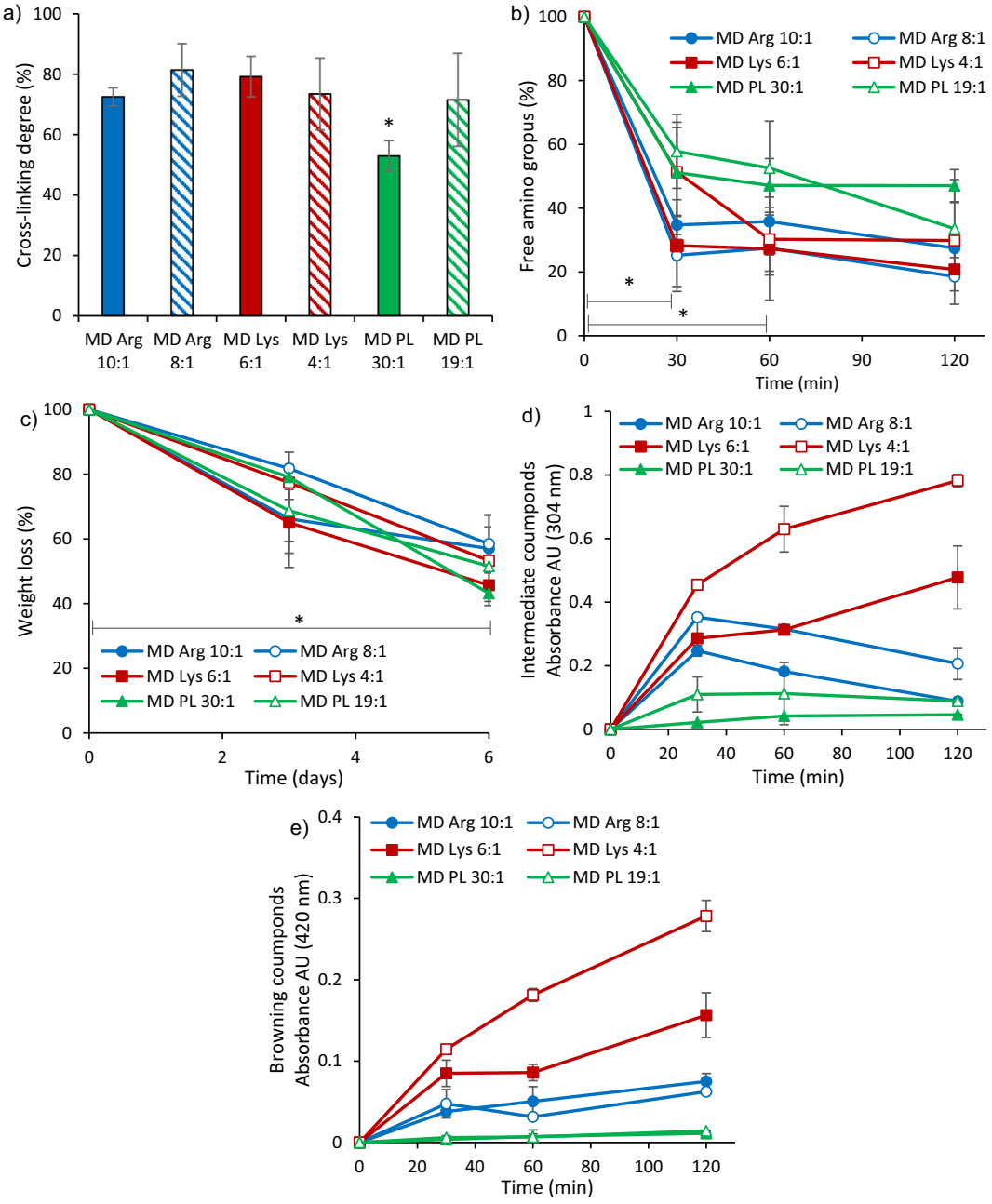

Fig. 4. a) Percentage (%) of free amino groups; b) cross-linking degree of scaffolds subjected to heating treatment after 120 min; c) scaffold in vitro degradation in PBS at 37 °C; d) absorbance profiles of Amadori (λ = 304 nm) and e) browning compounds (λ = 420 nm) vs time for scaffolds subjected to heating at 180 °C for 120 min (mean values ± sd; $n = 3$). Values * indicate significant differences ($p < 0.05$).

3.3. Determination of intermediate and browning compounds

Fig. 4d and e report the profiles of intermediate and browning compounds vs heating time at 180 °C during the cross-linking process (2 h). The heating process is fundamental to activate the Maillard-type reaction since at zero time the absorbance of scaffolds just after the electrospinning process is negligible both at 304 nm (corresponding to intermediate formation) and at 420 nm (corresponding to melanoidins, browning compounds).

The heating treatment after electrospinning caused the browning of scaffolds from white to yellow-brownish, suggesting that the reaction of MD with poly/amino acids resulted in a visual change of color with increasing heating time: this indicates that Maillard compounds were formed.

In particular, the formation of intermediate compounds is maximum after 30 min at 180 °C, possibly due to the ease of interaction between MD carbonyl groups and amino groups of poly/amino acids (Fig. 4d). In fact, both moieties do not have any steric hindrance, and this has a significant influence on the formation of intermediate compounds, which are the precursors of the browning ones. Longer treatment time causes a slight decrease in the absorbance probably due to the degradation of the intermediate compounds to browning ones, since their conversion to browning compounds is faster than their formation [31]. At the same time, the formation of browning compounds increased (Fig. 4e) until the end of the cross-linking process, suggesting that the cross-linking reactions occurred. This conceivably causes the formation of a polymeric structure, modifying the system solubility to give a rather insoluble system [7].

At both 304 and 420 nm, scaffolds based on Lys and Arg have the higher absorbance profiles at both weight ratios of MD:poly/amino acid, indicating that in these systems the heating treatment gave rise to a higher amount of intermediate and browning compounds. Lys is the most favorite with respect to Arg since Lys has a linear structure without any steric hindrance while Arg has a guanidinium group. PL shows the lowest profiles for intermediate and browning compounds, and this could be due to its polymeric structure: as soon as the Maillard-type reaction starts, it is possible that the polylysine structure becomes less flexible and less prone to further reactions [29,30]. Moreover, these results are consistent with the higher concentration of amino groups (Lys > Arg > PL) available following the Maillard-type reaction.

To confirm these remarks, the behavior of a scaffold based on pure MD, as negative control, was compared to the MD poly/amino acids scaffolds and the absorbances read at 304 or 420 nm, corresponding to the λ_{max} of intermediate and browning compounds, respectively, were 0.0215 AU (± 0.0012) and 0.0057 AU (±0.0008), not significantly different to the basal value (blank). Moreover, pure MD scaffold remained prone to fast solubilization also after the crosslinking (thermal treatment).

3.4. Mechanical properties

Fig. 5 shows the mechanical properties of the scaffolds (force at break mN, a–d; elongation %, b–e; Young's modulus mN·cm^2, c–f) in dry (a, b, c) or wet (d, e, f) conditions.

At the dry state, all membranes were resistant to break and highly elastic with a maximum deformation lower than 14.5%. Arg-based scaffolds had minimal deformability and highest Force at break: in particular, MD Arg 10:1 showed twofold value with respect to MD Arg 8:1. Lys based scaffolds were less deformable and highly elastic: MD Lys 6:1 scaffolds were more resistant (10 times) and elastic (2 times) compared to MD Lys 4:1, and also characterized by higher deformability. MD-PL systems were characterized by similar behavior, independently of PL content, with a maximum tensile force of about 29.4 mN, a maximum deformation of about 13.5% and a higher elasticity. Pure MD scaffold was characterized by good mechanical properties similar to those of the other scaffolds based on poly/amino acids (Fmax: 32.25 ± 3.44 mN; E: 8.56 ± 1.82%; YM: 267.61 ± 113.99 mN/mm^2), nevertheless the hydration caused a complete dissolution of the systems.

The hydration of the scaffolds dramatically altered the scaffold mechanical properties, causing a remarkable decrease in resistance to break and elasticity, and an increase in deformability. However, in hydrated state scaffolds containing a higher amount of poly/amino acids possessed a higher resistance to break. It is conceivable that the highest available amino groups the greatest the interaction with MD, leading to reinforced structure and a higher mechanical resistance.

Considering the morphology of the scaffolds after hydration (Fig. 1b), the presence of Arg and PL at higher concentration allowed to better maintain single fiber structure with minimal merging with the side fibers and this seems to lead to a higher Force at break and higher deformability. This is a critical point since the mechanical properties play a fundamental role during scaffold implant. The behavior in dry state is correlated to the scaffold capability to preserve its integrity during grafting while this upon hydration offers a prediction of the scaffold performance and fate upon grafting [1,20]. The mechanical properties should offer a sufficient biomechanical support during tissue restoration for cell adhesion and proliferation. It has been reported that low stiffness matrices are able to allow and facilitate cell migration, while soft systems encourage cell proliferation [32].

3.5. Surface zeta potential

Fig. 5g, h, and i show the pH dependence of the ζ for the cross-linked scaffolds. The apparent ζ vs. pH profiles were generally lower when MD amino/polyamino acids ratio was higher, and this was directly related to the concentration of basic poly/amino acids (Arg pKa 12.48; Lys pKa 10.53; PL pKa 10). All scaffolds were characterized by negative zeta potential in physiological fluids, and this could be related to the high cross-linking between MD and poly/amino acids, occurred during heating treatment to form Maillard-type reaction products: this process involved amino groups causing a decrease of free groups close to 80%. It has been reported that surface zeta potential influences cell adhesion and proliferation onto a surface [33]: negative zeta potential in the physiological environment (pH 7.4) seems to influence calcium metabolism, which regulates the wound healing process. In fact, calcium is involved in skin homeostasis and acts as a secondary messenger in several signaling cascades critical in wound healing, by regulating fibroblast proliferation and keratinocyte migration [34].

3.6. Direct and indirect antioxidant properties

During the inflammatory phase of the healing process, neutrophils and macrophages are attracted to the wound site and produce ROS which protect the wound from invading microorganisms. ROS have a positive effect on angiogenesis, reepithelization, cell migration and proliferation. However, high ROS concentration impairs skin cell proliferation and migration, and induce severe tissue damage [35]. The antioxidant properties are important to effectively tackle chronic lesions. These were characterized by a direct method, via DPPH assay, to highlight the antioxidant properties of the Maillard-type reaction products, and by an indirect method, via iron ions chelating properties, to underline the capability of the Maillard-type reaction products to reduce the concentration of Fe^{2+}, involved in the generation of free radicals from Fenton reactions.

The direct antioxidant activity was related to the capability of scaffolds to reduce the stable radical DPPH•. Fig. 6a reports the profiles of the DPPH scavenging activity of the scaffolds over time, while Fig. 6b shows the gallic acid equivalents vs time profiles.

The DPPH % decreased over time for all the scaffolds (Fig. 6a) while the concomitant gallic acid equivalents increased over time, suggesting that the antioxidant activity potentiated over time, conceivably due to the effect of the browning compounds released. Lys and Arg based scaffolds showed rapid onset of DPPH oxidation and gallic acid equivalents. Their efficiency should be a consequence of a higher content of browning compounds with respect to the PL based scaffolds. This seems to be related to the molecular weight of the Maillard-type reaction products: the higher their molecular weight, the more intense the antioxidant activity [36]. The indirect antioxidant activity was related to the capability of the scaffolds to chelate Fe^{2+}.

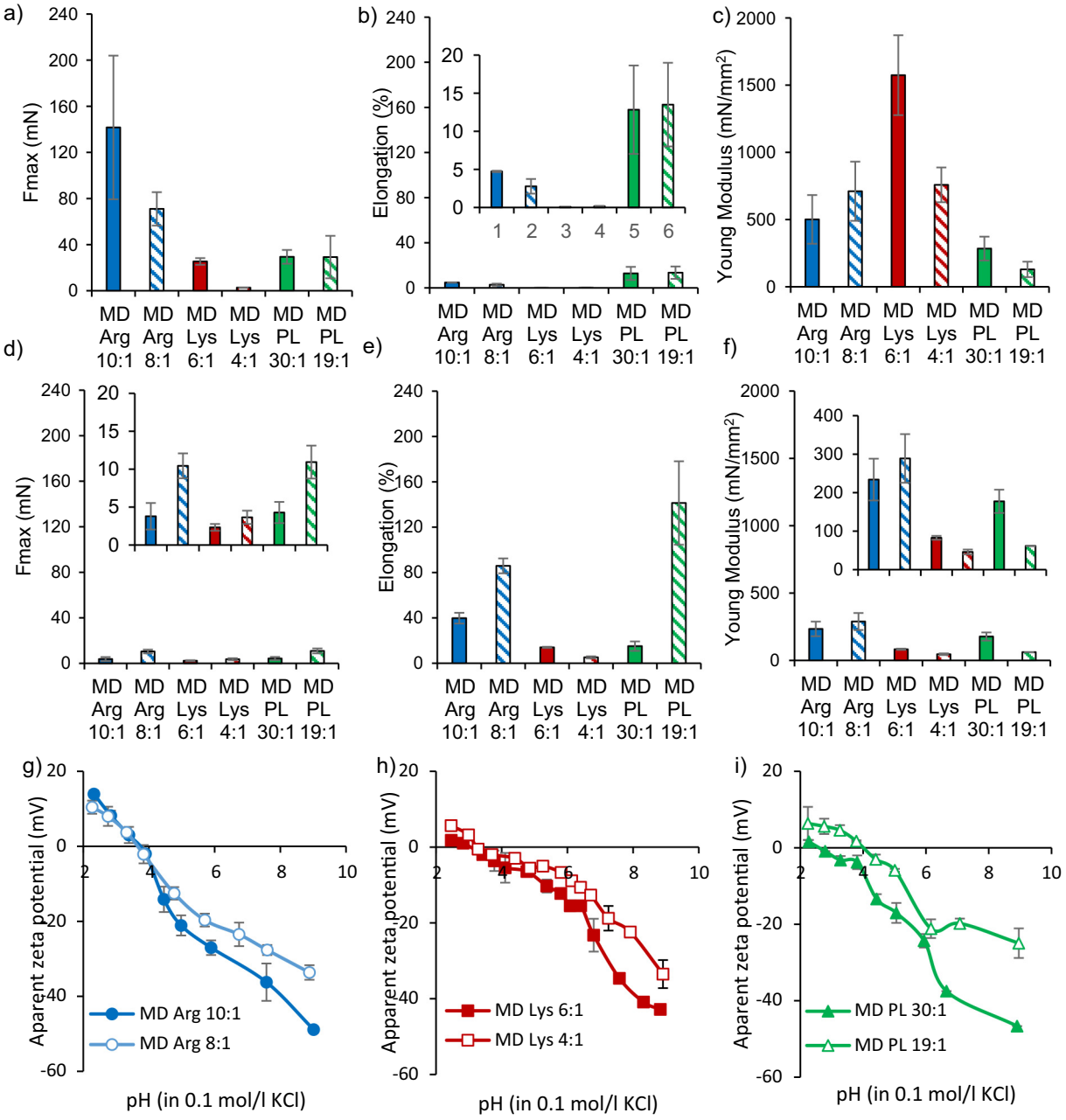

Fig. 5. Mechanical properties of scaffolds (a-d force at break mN; b-e elongation %, c-f Young Modulus mN.mm2) in the dry (a-c) or wet (d-f) state (mean values ± sd; $n = 3$). ANOVA one-way; Scheffé's test ($p \leq 0.05$): a) MD Arg 10:1 vs. MD Arg 8:1, MD Lys 6:1, MD Lys 4:1, MD PL 30:1, MD PL 19:1; b) MD Arg 10:1 vs. MD Lys 6:1, MD Lys 4:1; MD Lys 6:1 vs. MD PL 30:1, MD-PL 19:1; MD Lys 4:1 vs. MD PL 30:1, MD PL 19:1; c) MD Arg 8:1, MD Arg 10:1, MD Lys 6:1; MD Lys 4:1 vs. MD PL 19:1; d) MD Arg 10:1 vs. MD Arg 8:1, MD PL 19:1; MD Arg 10:1 vs. MD Lys 6:1, MD Lys 4:1; MD Lys 6:1 vs. MD PL 19:1; MD Lys 4:1 vs. MD PL 19:1; e) MD Arg 10:1 vs. MD PL19:1; MD Arg 8:1 vs. MD Lys 6:1, MD Lys 4:1, MD PL 30:1; MD Lys 6:1, MD Lys 4:1, MD PL 30:1 vs. MD PL 19:1; f) MD Arg 8:1 vs. MD Lys 6:1, MD Lys 4:1, MD PL 19:1. Zeta potential vs. pH profiles obtained for scaffolds (mean values ± s.d.; n = 3) of MD Arg (g), MD Lys (h), and MD PL (i). (mean values ± sd; $n = 6$).

In fact, Fe^{2+} plays a key role in oxidative stress processes: LIP undergoes redox cycling between its most stable oxidation states (Fe^{2+}/Fe^{3+}) and reacts with ROS, such as superoxide anion and hydrogen peroxide, giving rise to hydroxyl radicals via the Fenton reaction or superoxide-driven Fenton chemistry. The sequestration of Fe^{2+} results in increased VEGF (vascular endothelial growth factor) and HIF1-α (hypoxia-inducible factor) and has a positive effect on angiogenesis. In Fig. 6c, the profiles of the Fe^{2+} chelating activity of the scaffolds over time are reported, while Fig. 6d shows the EDTA equivalents vs time profiles. The Fe^{2+} percentage decreases over time for all the scaffolds (Fig. 6c) and parallelly the EDTA equivalents increased (Fig. 6d), suggesting that Fe^{2+} was sequestered by the scaffold activity-. This is conceivably due to the activity of the browning compounds released. Literature describes that Maillard-type reaction products are metal chelators and have high metal ion binding affinity. This behavior has been also related to the molecular weight of the Maillard reaction products: the higher the molecular weight of the Maillard-type reaction products the more intense the effect [37].

3.7. In vitro evaluation of scaffold

Fibroblasts have a crucial role in the wound healing process and, in particular, are fundamental for the extracellular matrix production. Fig. 7a reports the fibroblast cytocompatibility. All the concentrations of the extracts from scaffolds resulted cytocompatible towards fibroblasts with a cell viability

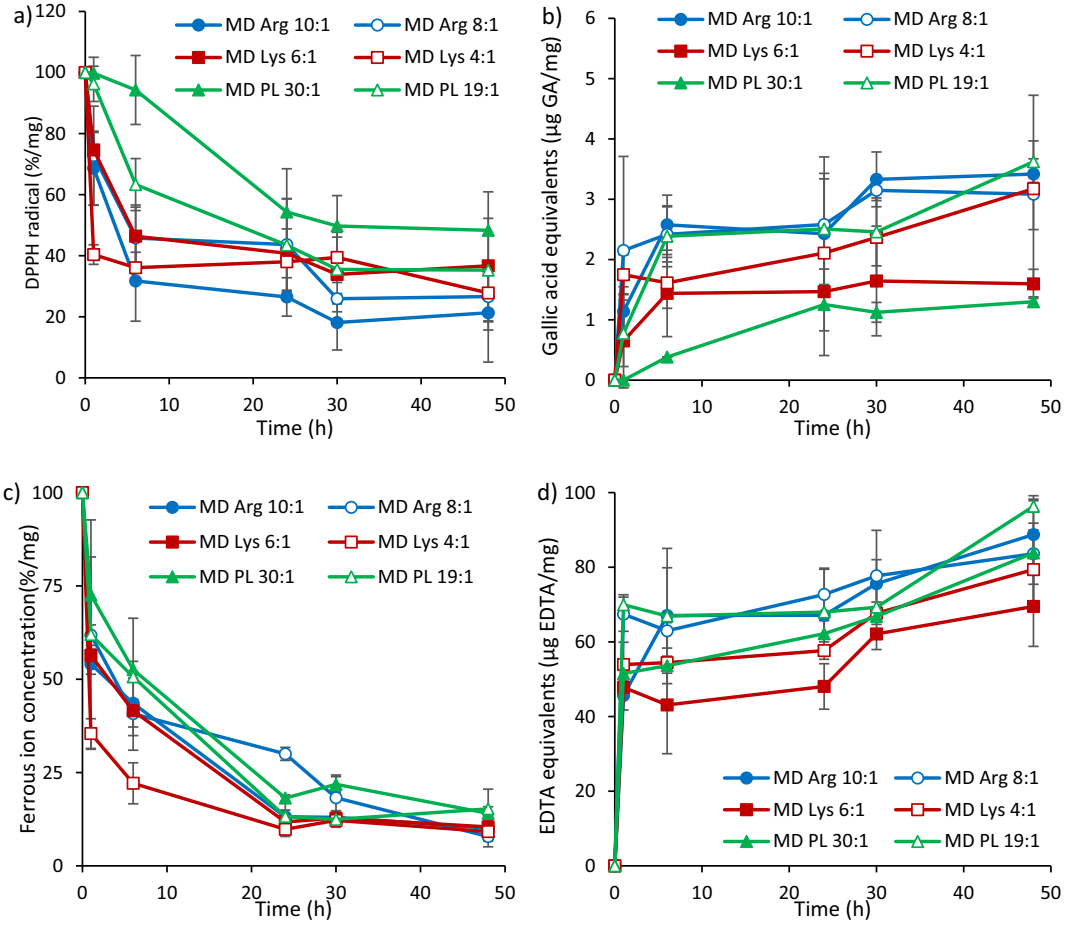

Fig. 6. a) DPPH scavenging activity of the scaffolds and b) gallic acid equivalents (mean values ± sd; $n = 3$) ANOVA one-way; Scheffé's test ($p \leq 0.05$): DPPH radical t_1: MD Lys 6:1 vs. MD Lys 4:1; MD Lys 4:1 vs. MD PL 30:1, MD PL 19:1; MD Arg 8:1; MD PL 30:1 vs. MD Arg 10:1; t_6: MD Lys 6:1 vs. MD PL 30; MD Lys 4:1 vs. MD PL 30:1; MD PL 30:1 vs. MD Arg 10:1, MD Arg 8:1; t_{24}, t_{30}, t_{48}: $p > 0.05$. Gallic acid equivalents t_1: MD PL 30:1 vs. MD Arg 8:1; t_6: MD Lys 6:1 vs. MD PL 30; MD Lys 4:1 vs. MD PL 30:1; MD PL 30:1 vs. MD Arg 10:1, MD Arg 8:1. c) Ferrous ion chelating activity of the scaffolds and d) EDTA equivalents. ANOVA one-way; Scheffé's test ($p \leq 0.05$): Ferrous ion concentration t_1: MD PL 30:1 vs. MD Lys 4:1; t6: MD PL 30:1 vs. MD Lys 4:1; MD PL 19:1 vs. MD Lys 4:1. EDTA equivalents t_6: MD Arg 10:1, MD Arg 8:1, MD PL 19:1 vs. MD Lys 6:1.

superimposable to that of the positive control (GM) (Fig. 7a). These results indicate that the scaffolds did not release cytotoxic components. It is conceivable that Maillard-type reaction products did not induce any cytotoxic effect. Similar results were obtained for scaffolds based on polycaprolactone functionalized via Maillard-type reaction [38]. Moreover, all the components and the scaffolds did not have cytotoxic effect towards macrophages (Fig. 7b) and did not cause a significant TNF- α secretion by the macrophages (Fig. 7c), significantly lower to that of LPS (positive control). This suggests that the scaffolds did not have a proinflammatory activity.

3.8. In vivo wound healing studies

All the scaffolds allowed wound closure with negligible wounded area at the end of the treatment. Lys seems to dramatically accelerate the process after 10 days of treatment (Fig. 8a).

The subcutaneous implant of the scaffolds allowed the evaluation of the scaffold safety. After 18 days from the implants (Fig. 8 d, e, f), neither residues of the scaffolds nor immune infiltrate were visible. The implant area was hardly recognized from the adjacent skin portions. Collagen distribution was superimposable to that of the intact skin, with perfectly reformed skin appendages (hair follicles and sebaceous glands). Moreover, PSR staining showed a continuous collagen layer, rich in orange-to-red fibers, with an identical pattern to that of intact skin. The histology of wounded tissue at the end of the treatment (18 days) showed that all the scaffolds were effective to induce skin healing upon injury (Fig. 8 g, h, i). In particular, riepithelization and accelerated collagen deposition were the key features. All the scaffolds induced a complete regeneration of the epithelium with a collagen fibers remodeling in orderly pattern while the lesions treated with physiological solution were characterized by a partial re-epithelialization and large amount of thin newly formed collagen fibers. Arg and Lys based scaffolds determined a complete restore of the skin epidermidis in multiple cell layers with a fair degree of keratinization. In the dermal tissue collagen was remodeled in an appropriated orientation to withstand the tensile stresses placed on the area of repair, suggesting an advanced stage of maturation and remodeling [39]. PSR staining indicates that almost all of the wound area were rich in collagen type III (green color). PL based scaffolds, on the contrary, still showed signals of the proliferative phase of healing, with a high number of blood vessels and a residual area of granulation tissue (a mixture of proliferating capillaries, fibroblast and inflammatory cells in a loose edematous extracellular matrix), denouncing a slightly delayed remodeling process in comparison with Arg and Lys based scaffolds. These could be related with the higher antioxidant activity of Arg and Lys based scaffolds. The lesions treated with physiological solution, were not completely re-epithelialized and presented a high vascular response, denouncing an earlier stage of healing.

4. Conclusion

In conclusion, electrospinning was successfully used to prepare scaffolds based on MD in association with poly/amino acids, starting from aqueous polymer blends.

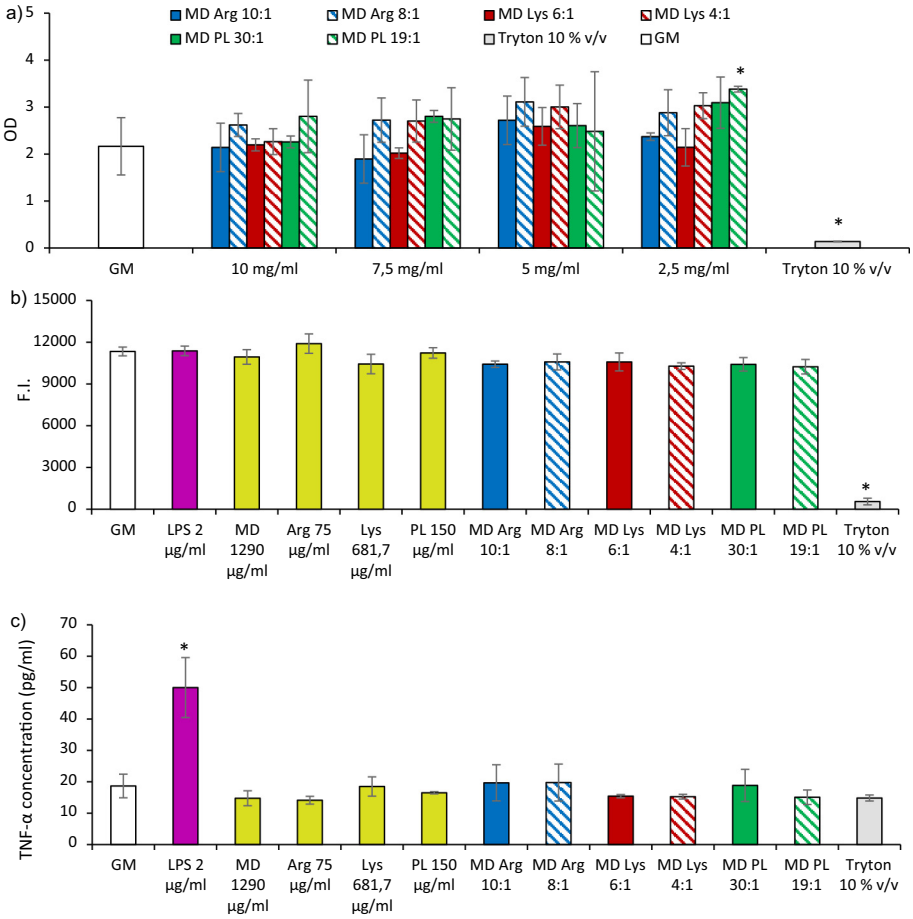

Fig. 7. a) Cell viability (OD - optical density) of fibroblasts after 24 h contact with the scaffold extracts at different dilutions; b) cytocompatibility of macrophages (F.I. - fluorescence intensity) of the scaffold components and the scaffolds after 24 h of contact and c) TNFα cytokine expression and concentrations (pg/mL) for cells exposed to components and to scaffolds (mean values ± sd; $n = 8$) (GM: growth medium; LPS: lipopolysaccharide) (mean values ± sd; n = 8). * indicates significant differences ($p < 0.05$).

The scaffolds designed and developed are based on maltodextrin, a polysaccharide, and poly/amino acids, scarcely immunogenic and cheap (compared to collagen) and were prepared by electrospinning using an innovative easy manufacture technique based on one step green process, without the employment of environmental hazardous chemicals (both solvent and crosslinker) and without safety issue for the clinical application. Cross-linking of the scaffolds was successfully obtained by heating via Maillard-type reaction and could be validated also as terminal sterilization: this enhances thermal stability. The scaffolds could store at room temperature in dry state. All these are advantageous features compared to those of the products on the market that are mainly based on collagen (an expensive material, potentially immunogenic) and are stored at refrigerated temperature (2–8 °C) and sterilized using gamma radiation.

The developed process allowed to obtain nanofibrous scaffolds with regular shape and smooth surface, preserved upon cross-linking and

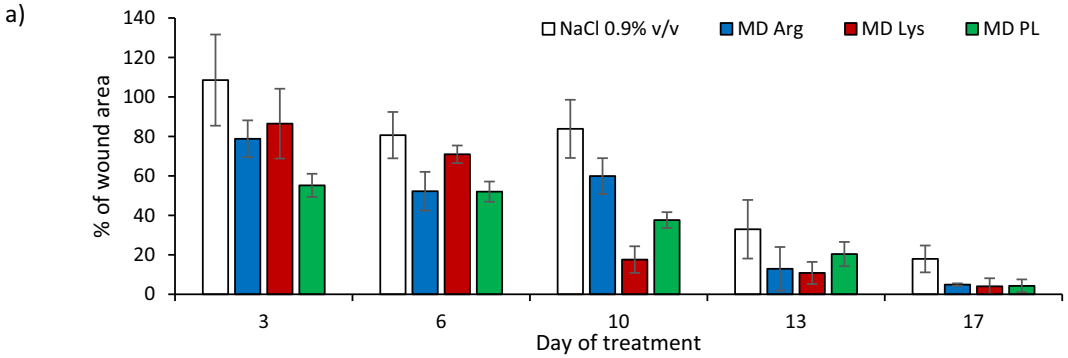

Fig. 8. a) Lesion area vs. time obtained during the treatments using MD Arg, MD Lys and MD PL scaffolds and saline solution (negative control) in an in vivo murine burn/excisional model (mean values ± sd; $n = 3$) and H&E and PSR sections of (b) lesion treated with saline solution as negative control, (c) intact skin, (d) subcutaneous implant of MD Arg scaffold, (e) subcutaneous implant of MD Lys scaffold, (f) subcutaneous implant of MD PL scaffold, (g) lesion treated with MD Arg scaffold, (h) lesion treated with MD Lys scaffold, (i) lesion treated with MD PL scaffold, Original magnification: Original magnification: 5×. Each micrograph frame has a width of 1780 µm.

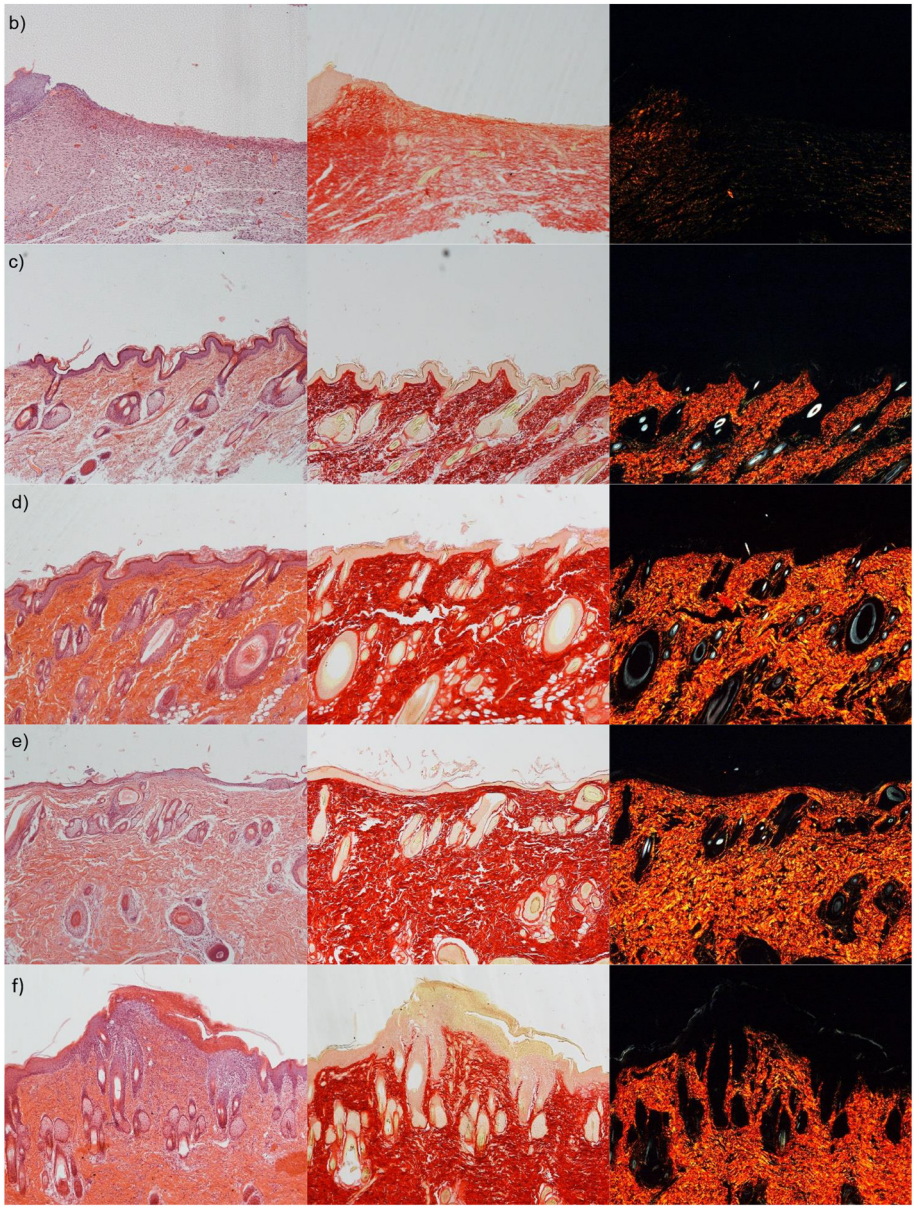

Fig. 8 (*continued*).

hydration. The Maillard-type reaction products conferred to the scaffolds distinctive properties as antioxidant ones. The preclinical in vitro results suggest that the scaffolds were biocompatible towards fibroblasts (highly involved in wound healing) and that those did not induce inflammation in a macrophages proinflammatory model.

Thanks to their safety and efficacy proved in a preclinical murine model, these scaffolds are promising devices for reparation of critical skin lesions.

CRediT authorship contribution statement

Marco Ruggeri: Data curation; Formal analysis; Methodology; Investigation; Visualization; Writing - original draft; Writing - review & editing. **Eleonora Bianchi:** Data curation; Formal analysis; Investigation. **Silvia Rossi:** Resources; Validation; Visualization. **Cinzia Boselli:** Formal analysis; Methodology; Investigation. **Antonia Icaro Cornaglia:** Formal analysis; Methodology; Investigation. **Lorenzo Malavasi:** Methodology; Investigation; Resources; Writing - review & editing. **Riccardo Carzino:** Methodology; Investigation; Writing - review & editing. **Giulia Suarato:** Writing – review & editing. **Rita Sánchez-Espejo:** Formal analysis; Methodology; Investigation. **Athanassia Athanassiou:** Methodology; Resources; Writing - review & editing. **Cesar Viseras:** Formal analysis; Methodology; Investigation. **Franca Ferrari:** Resources; Validation; Visualization. **Giuseppina Sandri:** Conceptualization; Data curation; Formal analysis; Funding acquisition; Investigation; Methodology; Project administration; Resources; Supervision; Validation; Roles/Writing - original draft; Writing - review & editing.

Declaration of competing interest

The authors declare that they have no known competing financial interests or personal relationships that could have appeared to influence the work reported in this paper.

Acknowledgements

Authors thank Horizon 2020 Research and Innovation Programme under Grant Agreement No. 814607, for funding the research project.

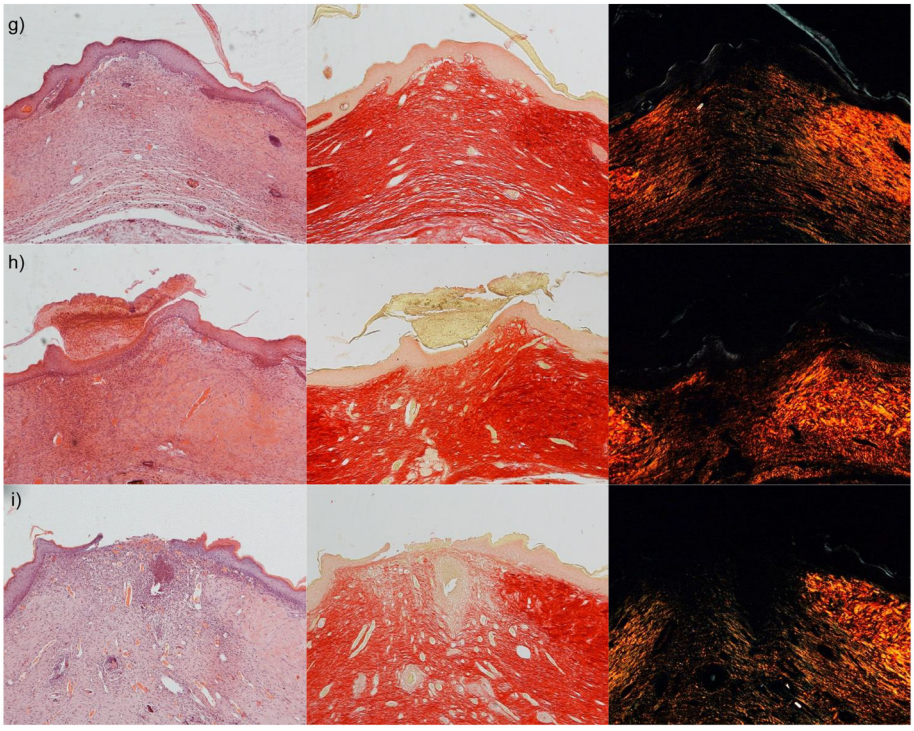

Fig. 8 (*continued*).

Appendix A. Supplementary data

Supplementary data to this article can be found online at https://doi.org/10.1016/j.msec.2021.112593.

References

[1] M. Ruggeri, E. Bianchi, S. Rossi, B. Vigani, M.C. Bonferoni, C. Caramella, G. Sandri, F. Ferrari, Nanotechnology-based medical devices for the treatment of chronic skin lesions: from research to the clinic, Pharmaceutics 27 (2020) E815.

[2] J.S. Boateng, K.H. Matthews, H.N. Stevens, G.M. Eccleston, Wound healing dressings and drug delivery systems: a review, J. Pharm. Sci. 97 (2008) 2892–2923.

[3] R.M. Salgado, O. Cruz-Castañeda, F. Elizondo-Vázquez, L. Pat, A. De la Garza, S. Cano-Colín, L. Baena-Ocampo, E. Krötzsch, Maltodextrin/ascorbic acid stimulates wound closure by increasing collagen turnover and TGF-β1 expression in vitro and changing the stage of inflammation from chronic to acute in vivo, J. Tissue Viability 26 (2017) 131–137.

[4] Z. Mohamed Amin, S.P. Koh, S.K. Yeap, N.S. Abdul Hamid, C.P. Tan, K. Long, Efficacy study of broken rice maltodextrin in vitro wound healing assay, Biomed. Res. Int. 2015 (2015), 687694.

[5] M.C.H. Azeredo, K.W. Waldron, Crosslinking in polysaccharide and protein films and coatings for food contact – a review, Trends Food Sci. Technol. 52 (2016) 109–122.

[6] A. Papetti, D. Mascherpa, G. Gazzani, Free α-dicarbonyl compounds in coffee, barley coffee and soy sauce and effects of in vitro digestion, Food Chem. 164 (2014) 259–265.

[7] A. Golkar, A. Nasirpour, J. Keramat, S. Desobry, Emulsifying properties of angum gum (Amygdalus scoparia Spach) conjugated to β-lactoglobulin through Maillard-type reaction, Int. J. Food Prop. 18 (2015) 2042–2055.

[8] F.J. Morales, S. Jimenez-Perez, Free radical scavenging capacity of Maillard reaction products as related to colour and fluorescence, Food Chem. 72 (2001) 119–125.

[9] S. Selvaraj, N.N. Fathima, Fenugreek incorporated silk fibroin nanofibers-a potential antioxidant scaffold for enhanced wound healing, ACS Appl. Mater. Interfaces 9 (2017) 5916–5926.

[10] J.A. Wright, T. Richards, S.K. Srai, The role of iron in the skin and cutaneous wound healing, Front. Pharmacol. 5 (2014) 156.

[11] A.G. Miller, S.J. Meade, J.A. Gerrard, New insights into protein crosslinking via the Maillard reaction: structural requirements, the effect on enzyme function, and predicted efficacy of crosslinking inhibitors as anti- ageing therapeutics, Bioorg. Med. Chem. 11 (2003) 843–852.

[12] M.N. Lund, C.A. Ray, Control of Maillard reactions in foods: strategies and chemical mechanisms, J. Agric. Food Chem. 65 (2017) 4537–4552.

[13] M.B. Witte, A. Barbul, Arginine physiology and its implication for wound healing, Wound Repair Regen. 6 (2003) 419–423.

[14] W. Liu, B. Tanasa, O.V. Tyurina, T.Y. Zhou, R. Gassmann, W.T. Liu, K.A. Ohgi, C. Benner, I. Garcia-Bassets, A.K. Aggarwal, A. Desai, P.C. Dorrestein, C.K. Glass, M.G. Rosenfeld, PHF8 mediates histone H4 lysine 20 demethylation events involved in cell cycle progression, Nature 466 (2010) 508–512.

[15] V. Mayandi, A.C. Wen, C. Choong, F.P. Dhand, T.T. Lim, H. Aung, N. Sriram, M.H. Dwivedi, S. Periayah, M. Sridhar, E.T.L. Fazil, G. Goh, R.W. Orive, T.M.S. Beuerman, X.J. Barkham, Z.X. Loh, V.A. Liang, S. Barathi, S.J. Ramakrishna, N.K. Chong, R. Lakshminarayanan Verma, Multifunctional antimicrobial nanofiber dressings containing ε-polylysine for the eradication of bacterial bioburden and promotion of wound healing in critically colonized wounds, ACS Appl. Mater. Interfaces 12 (2020) 15989–16005.

[16] Z. Tan, Y. Shi, B. Xing, Y. Hou, J. Cui, S. Jia, The antimicrobial effects and mechanism of ε-poly-lysine against Staphylococcus aureus, Bioresour. Bioprocess 6 (2019) 11.

[17] N.A. Patil, B. Kandasubramanian, Functionalized polylysine biomaterials for advanced medical applications: a review, Eur. Polym. J. 146 (2021), 110248.

[18] N. Castro, V. Durrieu, C. Raynaud, A. Rouilly, Influence of DE-value on the physico-chemical properties of maltodextrin for melt extrusion processes, Carb. Polym. 144 (2016) 464–473.

[19] M.M. Leane, R. Nankervis, A. Smith, L. Illum, Use of the ninhydrin assay to measure the release of chitosan from oral solid dosage forms, Int. J. Pharm. 271 (2004) 241–249.

[20] A. Faccendini, M. Ruggeri, D. Miele, S. Rossi, M.C. Bonferoni, C. Aguzzi, P. Grisoli, C. Viseras, B. Vigani, G. Sandri, F. Ferrari, Norfloxacin-loaded electrospun scaffolds: montmorillonite nanocomposite vs.free drug, Pharmaceutics 4 (2020) 325.

[21] G. Sandri, S. Rossi, M.C. Bonferoni, D. Miele, A. Faccendini, E.Del Favero, E.Di Cola, A.I. Cornaglia, C. Boselli, T. Luxbacher, L. Malavasi, F. Ferrari, L. Cantu', Chitosan/glycosaminoglycan scaffolds for skin reparation, Carbohydr. Polym. 220 (2019) 219–227.

[22] M. Budai-Szűcs, M. Ruggeri, A. Faccendini, A. Léber, S. Rossi, G. Varga, M.C. Bonferoni, P. Vályi, K. Burián, E. Csányi, G. Sandri, F. Ferrari, Electrospun scaffolds in periodontal wound healing, Polymers 13 (2021) 307.

[23] V.D. Jakovljević, J.M. Milićević, J.D. Stojanović, R.S. Solujić, M.M. Vrvić, Antioxidant activity of ethanolic extract of Penicillium chrysogenum and Penicillium fumiculosum, Hem. Ind. 68 (2014) 43–49.

[24] Y.Y. Lim, T.T. Lim, J.J. Tee, Antioxidant properties of several tropical fruits: a comparative study, Food Chem. 103 (2007) 1003–1008.

[25] G. Sandri, A. Faccendini, M. Longo, M. Ruggeri, S. Rossi, M.C. Bonferoni, D. Miele, A. Prina-Mello, C. Aguzzi, C. Viseras, F. Ferrari, Halloysite- and montmorillonite-loaded scaffolds as enhancers of chronic wound healing, Pharmaceutics 12 (2020) 179.

[26] C. Liang, F. Yuan, F. Liu, Y. Wang, Y. Gao, Structure and antimicrobial mechanism of ε-polylysine–chitosan conjugates through Maillard reaction, Int. J. Biol. Macromol. 70 (2014) 427–434.

[27] B. Vigani, S. Rossi, G. Sandri, M.C. Bonferoni, M. Rui, S. Collina, F. Fagiani, C. Lanni, F. Ferrari, Dual-functioning scaffolds for the treatment of spinal cord injury: alginate nanofibers loaded with the sigma 1 receptor (S1R) agonist RC-33 in chitosan films, Mar. Drugs 18 (2019) 21.

[28] Š. Horvat, A. Jakas, E. Vass, J. Samu, M. Hollósi, CD and FTIR spectroscopic studies of amadori compounds related to the opioid peptides, J. Chem. Soc. 2 (1997) 1523–1528.

[29] S.E. Lee, H. Chung, Y.S. Kim, Effects of enzymatic modification of wheat protein on the formation of pyrazines and other volatile components in the Maillard reaction, Food Chem. 131 (2012) 1248–1254.

[30] S. Wu, J. Hu, L. Wei, Y. Du, X. Shi, L. Zhang, Antioxidant and antimicrobial activity of Maillard reaction products from xylan with chitosan/chitooligomer/glucosamine hydrochloride/taurine model systems, Food Chem. 148 (2014) 196–203.

[31] I.G. Hwang, H.Y. Kim, K.S. Woo, J. Lee, H.S. Jeong, Biological activities of Maillard reaction products (MRPs) in a sugar–amino acid model system, Food Chem. 126 (2011) 221–227.
[32] B.M. Baker, B. Trappmann, W.Y. Wang, M.S. Sakar, I.L. Kim, V.B. Shenoy, A.J. Burdick, C.S. Chen, Cell-mediated fibre recruitment drives extracellular matrix mechanosensing in engineered fibrillar microenvironments, Nat. Mater. 14 (2015) 1262–1268.
[33] F. García-Villén, A. Faccendini, D. Miele, M. Ruggeri, R. Sánchez-Espejo, A. Borrego-Sánchez, P. Cerezo, S. Rossi, C. Viseras, G. Sandri, Wound healing activity of nanoclay/spring water hydrogels, Pharmaceutics 12 (2020) 467.
[34] A.B. Lansdown, Calcium: a potential central regulator in wound healing in the skin, Wound Repair Regen. 10 (2002) 271–285.
[35] M. Mittal, M.R. Siddiqui, K. Tran, S.P. Reddy, A.B. Malik, Reactive oxygen species in inflammation and tissue injury, Antioxid. Redox Signal. 20 (2014) 1126–1167.
[36] B. Ruiz-Roca, M.P. Navarro, I. Seiquer, Antioxidant properties and metal chelating activity of glucose-lysine heated mixtures: relationships with mineral absorption across Caco-2 cell monolayers, J. Agric. Food Chem. 56 (2008) 9056–9063.
[37] H. Jing, D.D. Kitts, Antioxidant activity of sugar-lysine Maillard reaction products in cell free and cell culture systems, Arch. Biochem. Biophys. 429 (2004) 154–163.
[38] D. Simões, S.P. Miguel, I.J. Correia, Biofunctionalization of electrospun poly (caprolactone) fibers with Maillard reaction products for wound dressing applications, React. Funct. Polym. 131 (2018) 191–202.
[39] A.J. Singer, R.A. Clark, Cutaneous wound healing, N. Engl. J. Med. 341 (1999) 738–746.